Complementary roles of tumour specific PET tracer ^{18}F-FAMT to ^{18}F-FDG PET/CT for the assessment of bone metastasis

Motoho Morita, Tetsuya Higuchi, Arifudin Achmad, Azusa Tokue, Yukiko Arisaka & Yoshito Tsushima

European Journal of Nuclear Medicine and Molecular Imaging

ISSN 1619-7070

Eur J Nucl Med Mol Imaging
DOI 10.1007/s00259-013-2487-7

Springer

Eur J Nucl Med Mol Imaging
DOI 10.1007/s00259-013-2487-7

ORIGINAL ARTICLE

Complementary roles of tumour specific PET tracer ^{18}F-FAMT to ^{18}F-FDG PET/CT for the assessment of bone metastasis

Motoho Morita · Tetsuya Higuchi · Arifudin Achmad · Azusa Tokue · Yukiko Arisaka · Yoshito Tsushima

Received: 7 March 2013 / Accepted: 11 June 2013

Abstract
Purpose The usefulness of ^{18}F-FDG PET/CT for bone metastasis evaluation has already been established. The amino acid PET tracer [^{18}F]-3-fluoro-alpha-methyl tyrosine (^{18}F-FAMT) has been reported to be highly specific for malignancy. We evaluated the additional value of ^{18}F-FAMT PET/CT to complement ^{18}F-FDG PET/CT in the evaluation of bone metastasis.
Methods This retrospective study included 21 patients with bone metastases of various cancers who had undergone both ^{18}F-FDG and ^{18}F-FAMT PET/CT within 1 month of each other. ^{18}F-FDG-avid bone lesions suspicious for malignancy were carefully selected based on the cut-off value for malignancy, and the SUVmax of the ^{18}F-FAMT in the corresponding lesions were evaluated.
Results A total of 72 ^{18}F-FDG-positive bone lesions suspected to be metastases in the 21 patients were used as the reference standard. ^{18}F-FAMT uptake was found in 87.5 % of the lesions. In the lesions of lung cancer origin, the uptake of the two tracers showed a good correlation (40 lesions, r=0.68, P<0.01). Bone metastatic lesions of oesophageal cancer showed the highest average of ^{18}F-FAMT uptake. Bone metastatic lesions of squamous cell carcinoma showed higher ^{18}F-FAMT uptake than those of adenocarcinoma. No significant difference in ^{18}F-FAMT uptake was seen between osteoblastic and osteolytic bone metastatic lesions.
Conclusion The usefulness of ^{18}F-FAMT PET/CT for bone metastasis detection regardless of the lesion phenotype was demonstrated. The fact that ^{18}F-FAMT uptake was confirmed by ^{18}F-FDG uptake suggests that ^{18}F-FAMT PET/CT has the potential to complement ^{18}F-FDG PET/CT for the detection of bone metastases.

Keywords Bone metastasis · Amino-acid PET tracer · ^{18}F-FAMT · ^{18}F-FDG · PET/CT

Introduction

Average life expectancy after the diagnosis of cancer has been extended with progress in early diagnosis and improved treatment of cancer [1]. Bone metastasis is commonly seen in 20–30 % patients with all types of cancer and its prevalence in breast and prostate cancer is up to 70 % [2]. Although bone metastasis may not be the direct cause of death from cancer, its presence directly affects the treatment strategy and thus affects the patient's prognosis. In addition, acute pain, morbid bone fracture and bone metastasis-related myelopathy significantly decrease the patient's quality of life. Thus, early and accurate detection of bone metastasis is important for adequate patient management [2, 3].

The current modalities available for bone metastasis detection include plain radiography, CT and MRI for anatomical imaging, and bone scintigraphy (BS) and PET for functional imaging [4]. Recently, whole-body screening for bone metastases has become possible using MRI with diffusion-weighted image background body signal suppression (DWIBS) [5]. BS

M. Morita
Department of General Medicine, Gunma University Hospital, Maebashi, Gunma, Japan

M. Morita (✉) · T. Higuchi · A. Achmad · A. Tokue · Y. Arisaka · Y. Tsushima
Department of Diagnostic Radiology and Nuclear Medicine, Gunma University Graduate School of Medicine, 3-39-22 Showa-machi, Maebashi, Gunma 371-8511, Japan
e-mail: motom-x@orion.ocn.ne.jp

A. Achmad
Department of Radiology, Faculty of Medicine, Gadjah Mada University, Yogyakarta, Indonesia

Published online: 05 September 2013

with ^{99m}Tc-methylene diphosphonate (^{99m}Tc-MDP) is a widely available functional imaging modality for initial whole-body screening for bone metastases. Whole-body ^{18}F-NaF PET, which can visualize elevated bone mineral metabolism around bone metastatic lesions, is also useful for whole-body screening for bone metastases, and has been reported to be more sensitive than BS [6–9]. ^{18}F-FDG PET/CT which visualizes elevated glucose metabolism is also useful in the evaluation of bone metastasis, as well as providing superior detection of the primary cancer lesion [10, 11]. However, ^{18}F-FDG also accumulates in inflammatory lesions, benign tumours and several normal organs, raising doubts about its ability to detect malignant lesions, particularly when this is added to the possibility of false-positive uptake. In addition, BS and ^{18}F-NaF PET are better for detecting osteoblastic lesions [6] while ^{18}F-FDG PET/CT is better for detecting osteolytic lesions [12], indicating that final results from these imaging modalities might be different depending on the type of bone metastasis.

Amino acid PET tracers that show more specific accumulation in cancer cells have been developed [13]. Both normal and neoplastic cells require amino acid transporters for growth and proliferation [14, 15]. Among these transporters, the L system, a Na^+-independent amino acid transport system, provides a major pathway into the cell for large neutral amino acids which comprise most of the essential amino acids, such as leucine, isoleucine, valine, phenylalanine, tyrosine, tryptophan, methionine and histidine [14, 16–18]. For its functional expression in the cell membrane, covalent association with the heavy chain of 4 F2 cell-surface antigen (4F2hc) is required [17]. Previous studies have demonstrated that L-amino acid transporter type 1 (LAT1), a member of the L-system amino acid transporter receptor family, is highly expressed in proliferating tissues including tumour cell lines and primary human tumours [18, 19]. Among the new amino acid analogue radiotracers, ^{11}C-methionine is the first that has been reported to be useful for bone metastasis detection and also provides better diagnostic utility than BS in the evaluation of bone metastasis [20].

In our facility, we have developed -3-[^{18}F]fluoro-alpha-methyl tyrosine (^{18}F-FAMT), an amino acid PET tracer [21], and have tested its potential usefulness in the detection of neoplasms using experimental tumour models [22]. The specific accumulation of ^{18}F-FAMT in malignant tumours has been evaluated in the clinical setting and has been shown to be useful for the diagnosis of various types of malignant tumour [23–29]. Clinical trials have also shown that ^{18}F-FAMT PET is useful for discriminating true malignant tumours from benign lesions and inflammatory sites [30, 31]. Wiriyasermkul et al. have confirmed the underlying molecular mechanism of this unique phenomenon, that ^{18}F-FAMT accumulates in tumour cells exclusively via LAT1 [32]. In this study, we analysed the additional usefulness of ^{18}F-FAMT PET/CT for the diagnosis of bone metastases as a complement to routine PET/CT with ^{18}F-FDG.

Materials and methods

Patients

This retrospective study included 21 patients (15 men and 6 women, age 55–81 years, mean 71 years) with advanced cancer complicated by bone metastasis who had undergone both ^{18}F-FDG PET/CT and ^{18}F-FAMT PET/CT between August 2010 and October 2011. The inclusion criteria were: (1) less than 1 month between the ^{18}F-FDG-PET/CT and FAMT-PET/CT scans, and (2) none of the metastatic lesions had received treatment. The study design was reviewed and approved by our institutional review board.

The primary tumours were as follows: lung carcinoma (nine patients), oesophageal carcinoma (six patients), prostate carcinoma (two patients), and one patient each with pancreatic carcinoma, cholangiocellular carcinoma, thymic carcinoma and stomach cancer (Table 1). In view of the stage of the tumours, none of the bone metastases could be confirmed histopathologically, and in all patients the diagnosis of bone metastasis was established from clinical follow-up, including physical signs, PET imaging, MRI, CT and BS (Table 2).

PET/CT studies

Both ^{18}F-FDG and ^{18}F-FAMT were synthesized in the cyclotron facility of Gunma University, with ^{18}F-FAMT produced according to the methods of Tomiyoshi et al. [21]. Patients were injected intravenously with ^{18}F-FAMT (5 MBq/kg, range 128.2–373.4 MBq, average 238.1 MBq) and ^{18}F-FDG (5 MBq/kg, range 200–375.2 MBq, average 276.7 MBq) after fasting for more than 6 h. PET/CT images were acquired 1 h (60±5 min) after injection using a Discovery STE PET/CT scanner (GE Healthcare, Milwaukee, WI) or a Biograph 16 PET/CT scanner (Siemens, Malvern, PA) with a 700-mm field of view (FOV) and a slice thickness of 3.27 mm. Three-dimensional (3-D) data acquisition was performed for 3 min per bed position, followed by image reconstruction with the 3-D ordered subsets expectation maximization method. Segmented attenuation was corrected by X-ray CT (140 kV, 120–240 mAs) to produce 128×128 matrix images. CT images were reconstructed using a conventional filtered back-projection method. Axial full-width at half-maximum (FWHM) at 1 cm from the centre of the FOV was 5.6 mm, and z-axis FWHM at 1 cm from the centre of the FOV was 6.3 mm. Intrinsic system sensitivity was 8.5 cps/kBq for 3-D acquisition. Both PET scanners were calibrated regularly with a phantom, and their SUV accuracy was routinely evaluated to ensure that the SUV

Table 1 Characteristics of the patients and their positive lesions seen on ^{18}F-FDG and ^{18}F-FAMT

No.	Age (years)	Sex	Primary tumour	Histopathological phenotype	^{18}F-FDG-positive lesions (*n*)	^{18}F-FAMT-positive lesions (*n*)
1	60	F	Lung	Adenocarcinoma	6	6
2	80	F	Lung	Adenocarcinoma	1	0
3	70	M	Oesophagus	Squamous cell carcinoma	1	0
4	66	F	Lung	Non-small-cell	3	2
5	65	M	Oesophagus	Squamous cell carcinoma	1	0
6	77	M	Stomach	Endocrine cell carcinoma	1	1
7	79	M	Lung	Unknown	2	2
8	55	F	Oesophagus	Squamous cell carcinoma	2	2
9	60	M	Oesophagus	Squamous cell carcinoma	1	1
10	70	M	Lung	Adenocarcinoma	2	1
11	62	F	Bile duct	Cholangiocellular carcinoma	1	1
12	73	M	Pancreas	Adenocarcinoma	1	1
13	66	M	Lung	Squamous cell carcinoma	5	5
14	72	M	Thymoma	Sarcomatoid carcinoma	3	3
15	76	F	Lung	Adenocarcinoma	4	3
16	80	M	Lung	Small-cell and squamous cell carcinoma	6	4
17	73	M	Lung	Large-cell neuroendocrine carcinoma	11	11
18	81	M	Oesophagus	Squamous cell carcinoma	2	2
19	72	M	Prostate	Adenocarcinoma	2	1
20	76	M	Oesophagus	Squamous cell carcinoma	8	8
21	73	M	Prostate	Adenocarcinoma	9	9

values produced were comparable. Patients were scanned from the thigh to the head in the arms-down position. No intravenous contrast material was administered for CT scanning. Limited breath-holding at normal expiration was used during CT to avoid motion-induced artefacts and allow coregistration of CT and PET images in the area of the diaphragm.

PET/CT images acquired using ^{18}F-FDG and ^{18}F-FAMT were interpreted independently by two experienced nuclear medicine physicians (M.M., T.H.) and were analysed using an AW Workstation (GE Healthcare) and e.soft (Siemens). The resolution of the reconstructed images was approximately 5 mm at FWHM. Colour display with the rainbow or hot iron scale with the SUV window of 0 to 5 was used. Both interpreting physicians were blinded to the patients' data and clinical history. Discrepant interpretations of the two readers were resolved by consensus. For semiquantitative analysis of tumour uptake of the tracers, rectangular and box-shaped 3-D regions of interest (ROI) were manually drawn around the rim of the tumour lesion and placed over the area showing the highest uptake of tracer in the tumour. SUVmax, which was defined as the peak SUV on the pixel with the highest count within the ROI, were calculated using the following formula:

$$\mathrm{SUV} = \frac{\text{Radioactive concentration in the ROI } \left(\text{MBq}/\text{g}\right)}{\left[\text{Injected Dose (MBq)} \Big/ \text{Patient's Body Weight (g)}\right]}$$

Side-by-side image review and analysis were performed to confirm that the SUVmax was derived from the same lesion on the baseline and follow-up scans. For the evaluation of the difference in ^{18}F-FDG and ^{18}F-FAMT uptakes in different categorical groups, ^{18}F-FAMT SUVmax to ^{18}F-FDG SUVmax ratios (FAMT/FDG SUVmax ratios) were calculated to describe the relative uptake of ^{18}F-FAMT compared with that of ^{18}F-FDG, since absolute uptake of ^{18}F-FAMT is usually much lower than that of ^{18}F-FDG.

^{18}F-FDG PET/CT images were initially reviewed for each patient to screen the extent of bone metastases. Each lesion for which the uptake on the ^{18}F-FDG PET/CT image was visually interpreted as abnormal and exceeding the cut-off value for malignancy (SUVmax ≥1.9) was confirmed with

Table 2 Patient monitoring methods

Monitoring	No. of patients
Physical signs + ^{18}F-FDG PET/CT	14
Physical signs + ^{18}F-FDG PET/CT + bone scintigraphy	3
Physical signs + ^{18}F-FDG PET/CT + MRI	2
Physical signs + ^{18}F-FDG PET/CT + bone scintigraphy + MRI	1
Physical signs only	1

its corresponding presence on the ^{18}F-FAMT PET/CT image [33]. The bone metastases were morphologically evaluated (osteoblastic or osteolytic type) using the CT images. If the final classification was difficult, the diagnosis of either osteoblastic or osteolytic metastasis was made based on the CT finding of the lesion where ^{18}F-FDG uptake was prominent.

Statistical analysis

The correlation between ^{18}F-FDG and ^{18}F-FAMT uptakes in the bone metastatic lesions were evaluated by linear regression analysis between different categorical groups (primary lesion origin, histopathological type of the primary lesion and bone metastatic pathological phenotype). The Mann-Whitney *U* test was performed to evaluate the differences between SUVmax of ^{18}F-FAMT and ^{18}F-FDG. Student's *t* test and Welch's *t* test for two samples with unequal variance were performed to evaluate whether the two PET radiotracers accumulated differently in adenocarcinoma (AC) and squamous cell carcinoma (SCC) lesions, and in osteoblastic and osteolytic lesions. For all statistical analyses, *P* values less than 0.05 were considered statistically significant.

Results

The three major primary lesion origins of 72 bone metastatic lesions found on ^{18}F-FDG PET/CT scans were the lung, oesophagus and prostate. Among these lesions, 63 (87.5 %) also showed abnormal accumulation on ^{18}F-FAMT PET/CT images. Only one false-positive uptake was observed on ^{18}F-FAMT PET/CT, whereas 38 false-positive uptakes were observed on ^{18}F-FDG PET/CT, including degenerative changes in the joints. Thus the specificity of ^{18}F-FAMT PET/CT was 97.4 %. The accumulation of ^{18}F-FDG was significantly higher than that of ^{18}F-FAMT ($P<0.000$; mean SUVmax 5.871±3.04 vs. 1.804±0.85; as shown in Fig. 1). Since the variance of ^{18}F-FDG SUVmax was much higher than that of ^{18}F-FAMT SUVmax (Fig. 2a; 9.36 vs. 0.72), correlation between the SUVmax of the two radiotracers should be interpreted carefully ($r=0.26$, $P=0.027$). However, a high correlation between SUVmax of ^{18}F-FDG and that of ^{18}F-FAMT was found for bone metastases of lung cancer origin ($n=40$, $r=0.68$, $P<0.01$), while similar results were not observed for metastases of oesophageal cancer ($n=15$, $r=0.44$) nor for those of prostate cancer ($n=11$, $r=0.13$; Fig. 2b).

^{18}F-FAMT accumulated differently in bone metastases of lung, oesophageal and prostate cancer (Fig. 3). FAMT/FDG SUVmax ratio of bone metastasis from oesophageal cancer was the highest (0.59), followed by that from prostate cancer and lung cancer (0.50 and 0.26, respectively). Neither SCC type ($n=20$) nor AC type ($n=25$) tumours exhibited meaningful correlations between SUVmax of ^{18}F-FDG and ^{18}F-FAMT uptakes (data not shown). However, the accumulation of ^{18}F-FAMT in SCC type tumours was significantly higher than in AC type tumours (mean FAMT/FDG SUVmax ratio 0.52 vs. 0.35, $P<0.05$; Fig. 4). Figure 5 shows the analysis based on the bone metastasis phenotype. ^{18}F-FDG uptake was higher in the 10 osteolytic lesions than the 31 osteoblastic lesions ($t=2.13$, $P<0.05$), while on the contrary, the accumulation of ^{18}F-FAMT was not different in these two distinct bone metastasis phenotypes.

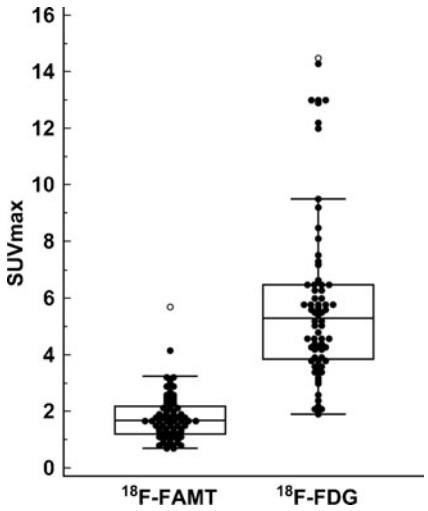

Fig. 1 ^{18}F-FDG and ^{18}F-FAMT SUVmax in 72 bone metastatic lesions with positive ^{18}F-FDG uptake. The average SUVmax for ^{18}F-FDG and ^{18}F-FAMT were 5.87±3.04 and 1.80±0.85, respectively, and ^{18}F-FDG showed significantly higher uptake ($P<0.01$)

Figure 6 shows the typical patterns of tracer accumulation in osteolytic and osteoblastic bone metastases, and also in degenerative changes. Osteoblastic bone metastases showed tracer uptakes on BS, ^{18}F-FDG PET/CT and ^{18}F-FAMT PET/CT. On the other hand, osteolytic bone metastases were not detected by BS, although positive uptake was noted on both ^{18}F-FDG and ^{18}F-FAMT. False-positive tracer uptake in degenerative change lesions were noted on BS and ^{18}F-FDG PET/CT, while true-negative on ^{18}F-FAMT PET/CT as no ^{18}F-FAMT uptake was observed, indicating its high specificity.

Typical findings of multiple bone metastasis in a patient with advanced lung cancer evaluated using ^{18}F-FDG and ^{18}F-FAMT PET/CT are presented on Fig. 7. Although ^{18}F-FDG uptake was more prominent than that of ^{18}F-FAMT, visualization of lesions on ^{18}F-FAMT PET/CT images provided adequate information to determine true malignancy. On PET/CT fusion images, accumulation of ^{18}F-FDG tended to spread more widely onto adjacent unaffected bone, resulting in an apparently larger tumour size compared to the original bone lesion. ^{18}F-FAMT accumulation, by contrast, provided a more precise size approximation to the original bone lesion seen in CT. Additionally, higher contrast as a result of the lack of nonspecific uptake was observed in the mediastinum and pelvic region.

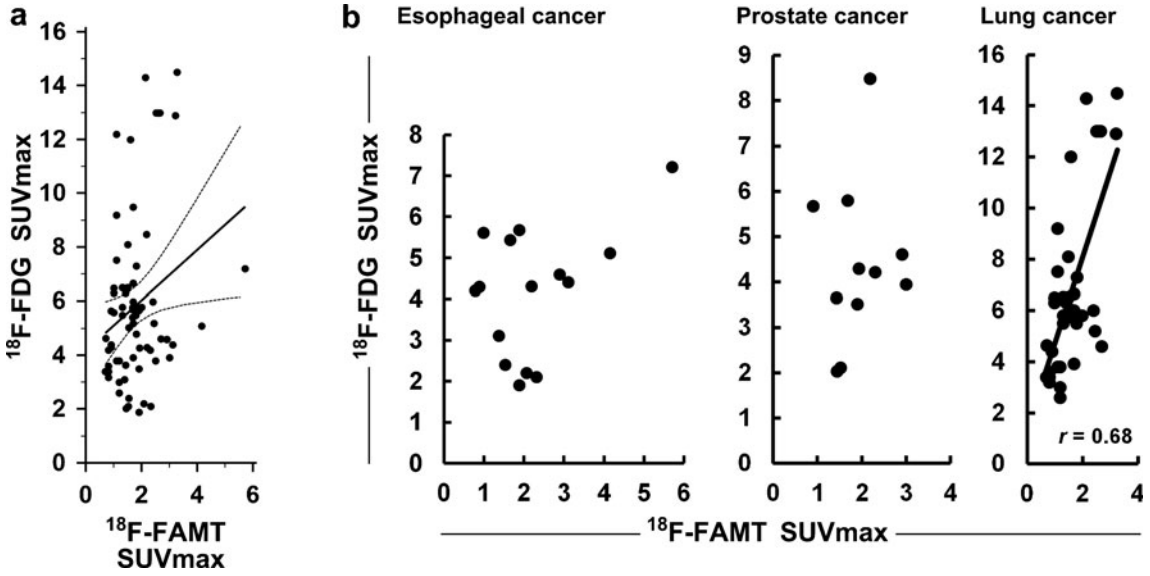

Fig. 2 Distribution of ^{18}F-FDG and ^{18}F-FAMT SUVmax and their correlation analysis for in all 72 lesions (r=0.26, P=0.027) (**a**), and based on the three major tumour origins (**b**). The *dotted lines* in **a** represent the range of values with a 95 % confidence of the true correlation coefficient

Discussion

In this study, as a complement to the current standard ^{18}F-FDG PET/CT for evaluation of malignant lesions, ^{18}F-FAMT PET/CT was able to successfully detect most of the bone metastases from various primary tumours. The FAMT/FDG uptake ratios depended on the tumour origin, tumour pathological type and bone metastatic type, and this additional information helped the further characterization of these lesions. It is well established that physiological and nonspecific uptake in organs and sites with a high rate of glucose metabolism such as the brain, heart and inflammatory is common in ^{18}F-FDG PET images. Instead of providing high specificity for malignancy, this drawback limits the ability of ^{18}F-FDG PET to discriminate inflammation and benign tumours from malignant lesions [10, 34]. In cancer patients, who largely comprise the elderly, this limitation potentially has significant consequences. Particularly in bone, accumulation of ^{18}F-FDG in the degenerative change lesions such as compression fractures from osteoporosis, osteoarthritis and inflammatory joint diseases often leads to difficulty in the detection of metastatic lesions [35]. On the contrary, physiological uptake of ^{18}F-FAMT is limited only to the urinary tract which is its excretion route.

Specific accumulation of ^{18}F-FAMT in malignant cells provided clear localization of true malignant lesions. This unique property is facilitated by ^{18}F-FAMT's exclusive

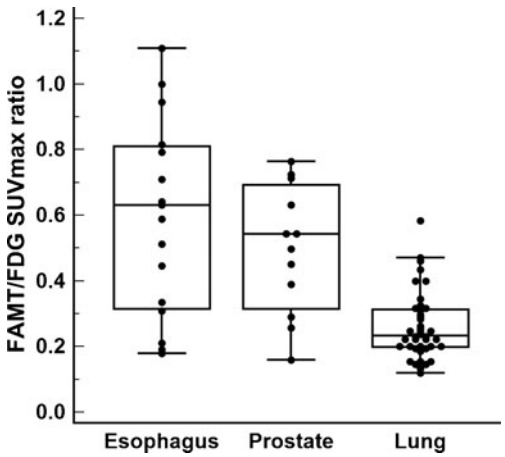

Fig. 3 FAMT/FDG SUVmax ratios of bone metastatic lesions based on their primary tumour origin

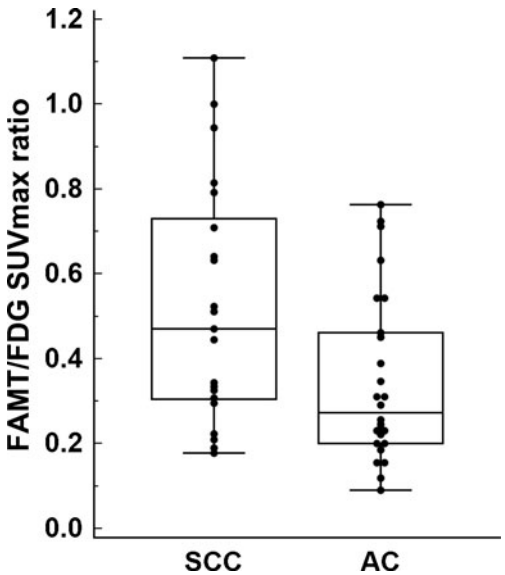

Fig. 4 FAMT/FDG SUVmax ratios of bone metastatic lesions based on their histopathological type

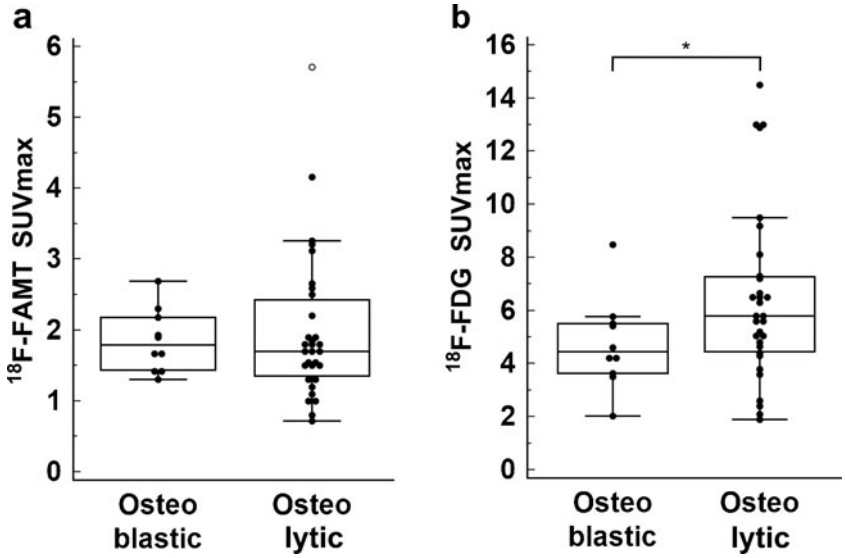

Fig. 5 SUVmax of ^{18}F-FAMT and ^{18}F-FDG based on the bone metastatic lesion phenotype.*$P<0.05$

internalization in cancer cells through the LAT1 receptor, and not by other L system receptors such as LAT2, which is widely expressed in normal cells [18, 32]. Therefore, nonspecific accumulation of ^{18}F-FAMT in normal organs is not observed. As a result, ^{18}F-FAMT PET/CT provides a high lesion-to-background contrast ratio, leading to the accurate diagnosis of malignancy in various tumour types [24–26, 28, 30, 31], particularly those in the brain [23, 29]. Compared to ^{18}F-FDG avidity which often spreads to adjacent tissues around malignancy because of uptake by macrophages and granulation tissue [36], uptake of ^{18}F-FAMT is low and restricted to the actual site of malignant cells. This additional

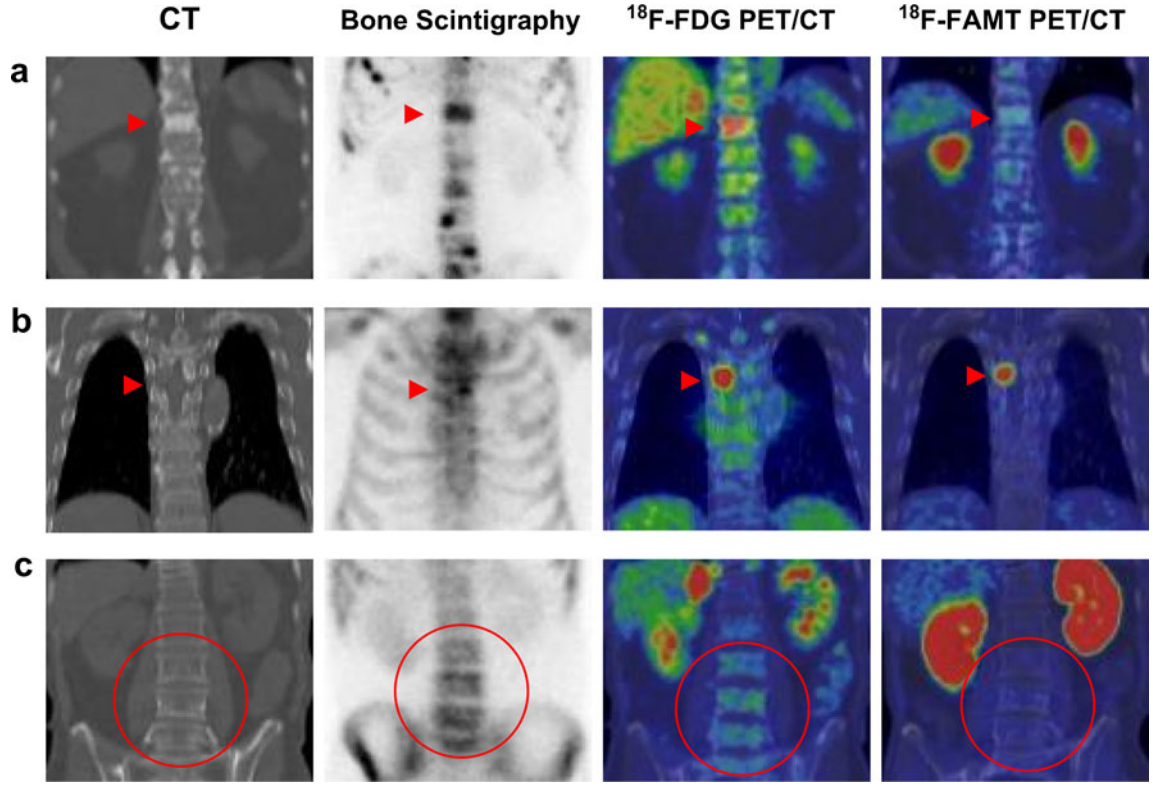

Fig. 6 Characteristic findings of osteoblastic (**a**) and osteolytic (**b**) bone metastases and degenerative changes (**c**). The osteoblastic lesion in patient 21 (**a**) shows tracer uptake on the BS, ^{18}F-FDG PET/CT and ^{18}F-FAMT PET/CT images, while the osteolytic lesion in patient 20 (**b**) shows no uptake on the BS image, although positive uptake is apparent on both the ^{18}F-FDG PET/CT and ^{18}F-FAMT PET/CT images. The degenerative change lesion in patient 14 (**c**) shows uptakes on both the BS and ^{18}F-FDG PET/CT images, while the ^{18}F-FAMT PET/CT image shows clear background with no uptake in the lesion area

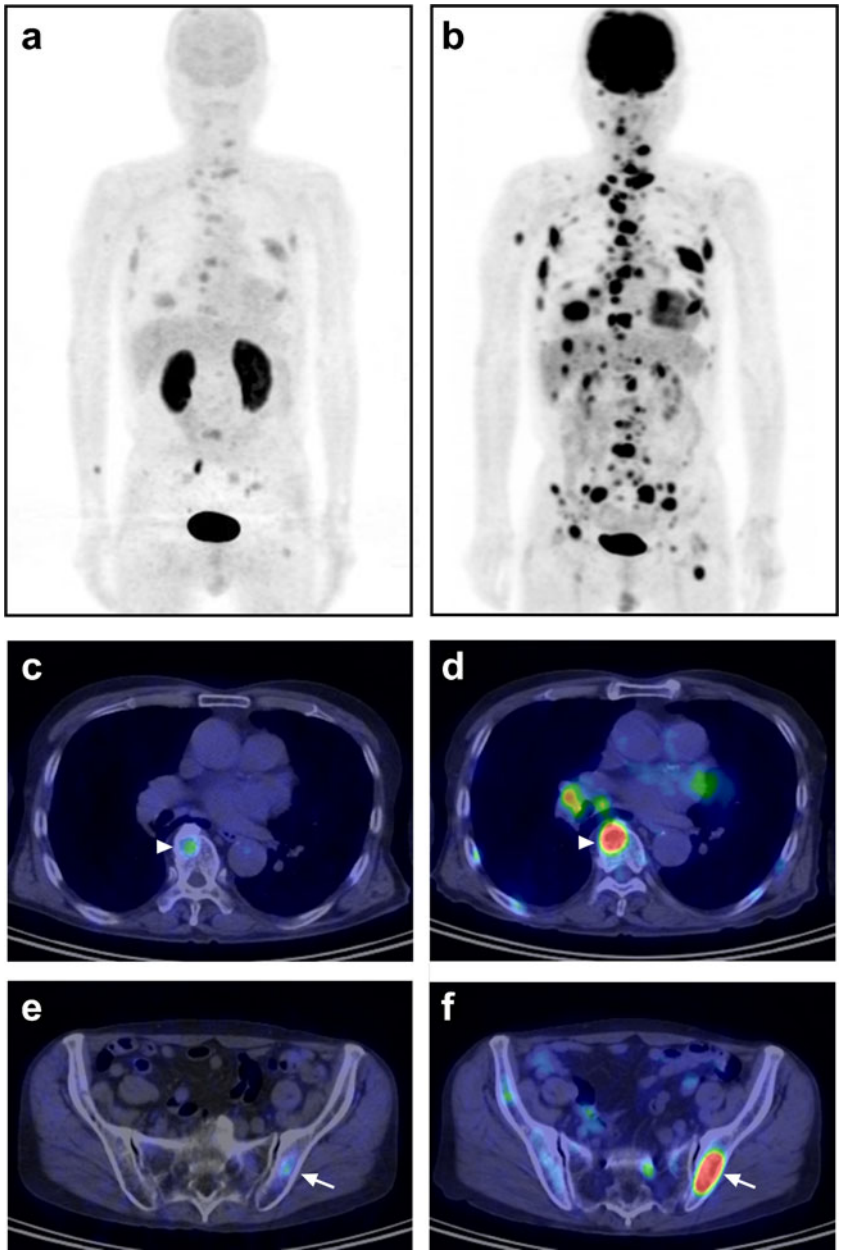

Fig. 7 A 73-year-old man with a diagnosis of lung cancer (patient 17) examined with ^{18}F-FAMT PET/CT (*left column*) and ^{18}F-FDG PET/CT (*right column*). **a**, **b** Whole-body PET MIP images show multiple metastatic bone lesions. ^{18}F-FAMT uptake (**a**) shows adequate contrast to confirm each of the malignant lesions despite being lower than ^{18}F-FDG uptake (**b**). **c**, **d** Axial PET/CT images at the thoracic level show limited ^{18}F-FAMT uptake in the thoracic spine (**c**, *arrowhead*) but prominent ^{18}F-FDG uptake at the same site (**d**, *arrowhead*). **e**, **f** Axial PET/CT images at the pelvic level also show limited ^{18}F-FAMT uptake in the left iliac bone (**e**, *arrow*) while ^{18}F-FDG uptake is spread more widely and is more intense (**f**, *arrow*). However, ^{18}F-FAMT PET/CT images show no nonspecific uptake in the mediastinum, lower abdomen and right iliac bone

value suggests the potential use of ^{18}F-FAMT for the accurate measurement of tumour dimensions which might be an advantage in monitoring response to therapy.

We observed different ^{18}F-FAMT uptake in bone metastatic lesions of different primary tumour origins. Bone metastases from oesophageal tumours, which is also SCC type as well as its primary, showed the highest uptake. It has been reported that high accumulation of ^{18}F-FAMT in SCC is due to their high expression of LAT1 [26, 28, 32]. Our findings suggest that squamous cells tend to have higher LAT1 expression than other cell types, but this early hypothesis needs to be confirmed in further studies.

In this study, we obtained clear and prominent ^{18}F-FAMT uptake in bone metastases regardless of their nature, osteolytic or osteoblastic. Interestingly, until recently no single imaging modality available had the ability to detect bone metastasis foci with high sensitivity and specificity regardless of the bone lesion phenotype. BS and SPECT with ^{99m}Tc-MDP is highly dependent on bone turnover, and therefore it is known for its superiority in detecting osteoblastic lesions but limited ability in detecting pure osteolytic lesions. Both modalities also have limited specificity and are unable to differentiate the early stage of bone metastasis from healing fractures, benign tumours and degenerative disease [37, 38]. On the other hand, even though ^{18}F-NaF PET/CT has higher accuracy than BS and SPECT, its lesion uptake reflects blood flow and osteoblastic activity, and therefore evaluation of osteolytic lesions requires careful examination for osteoblastic activity surrounding the lesion [40].

Confirmation of ^{18}F-NaF PET findings with CT and MRI is inevitable [6].

CT and MRI only are impractical for the detection of bone metastases, which makes their routine use for this indication unlikely at the present time [10, 37, 38]. A novel MRI technique, DWIBS, has been reported to be useful for the detection of bone metastases, but its sensitivity and specificity regarding bone lesion phenotype has not yet been evaluated [5, 39]. Despite its ability to detect bone metastases earlier than other modalities by targeting the glucose metabolism increase, ^{18}F-FDG PET/CT has low sensitivity in detecting osteoblastic lesions [12, 40, 41]. Our results also confirmed that ^{18}F-FDG accumulates differently in osteoblastic and osteolytic lesions. In contrast, similar uptake of ^{18}F-FAMT in the two distinct bone lesion phenotypes suggests that ^{18}F-FAMT PET/CT could be used for the detection of bone metastases of either phenotype. However, further investigation in larger studies is warranted. Related to bone structure remodelling, the cytokines RANKL, RANK and OPG have recently been reported to play an important role in the osteolytic process of bone metastasis [42]. Although the relationship between ^{18}F-FAMT uptake and proliferative activity evaluated by LAT1 expression in immunohistochemical specimens has already been reported [27], the relationship between these cytokines and LAT1 expression is still unclear and needs further study.

Currently, contrast-enhanced CT is used for radiation therapy planning, while ^{18}F-FDG PET/CT is used to obtain the metabolic information within the lesions during monitoring of therapeutic efficacy [43, 44]. However, it has been reported that following conventional radiation therapy or heavy-ion therapy, ^{18}F-FDG PET/CT is unable to distinguish recurrence or radiation necrotic lesions from secondary changes [28]. On the other hand, compared to ^{18}F-FDG, the absence of accumulation at inflammatory sites and its high specificity for malignancy are advantages of ^{18}F-FAMT [28], which might be expected to allow accurate detection of early response to radiation therapy. This potential of ^{18}F-FAMT PET/CT as a monitoring tool for radiation therapy efficacy requires further prospective study.

Due to the patients' advanced stage disease, obtaining histopathological confirmation of all bone metastatic lesions is impractical and is unethical when there is no impact on clinical management. Therefore, the main limitation of this study was that our ^{18}F-FAMT PET/CT findings were not rigorously verified by histopathological examination. Instead, bone metastasis was confirmed by careful examination and interpretation of the imaging and clinical follow-up. As shown in Table 2, most of the patients (20/21) were followed using ^{18}F-FDG PET/CT as well as clinically, and in six patients additional BS and/or MRI were also performed for monitoring purpose. Thus, the accuracy of the final clinical diagnosis for bone metastasis was considered to be reasonable. However, to provide robust evidence that ^{18}F-FAMT has true potential to replace histopathological confirmation of bone metastasis when biopsy or surgery is clinically inappropriate, further evaluation with post-mortem histopathological confirmation is warranted. In general, further clinical study with larger numbers of patients is essential to confirm these preliminary findings.

Conclusion

In this study, the usefulness of ^{18}F-FAMT PET/CT for the detection of bone metastases regardless of the bone lesion phenotype was demonstrated. The fact that ^{18}F-FAMT uptake was confirmed by ^{18}F-FDG uptake in bone metastatic lesions with higher lesion-to-background ratio suggests that ^{18}F-FAMT PET/CT has potential for use as a complement to ^{18}F-FDG PET/CT for accurate detection of bone metastases.

Acknowledgments The authors thank Professor Junichi Tamura and Associate Professor Yoshio Ohyama of the Department of General Medicine, Professor Hiroshi Koyama of the Department of Public Health, Professor Hiroyuki Kuwano and Dr. Tatsuya Miyazaki of the Department of General Surgical Science, and Dr. Kyoichi Kaira of the Oncology Center, Gunma University, for their generous support of this clinical study.

Conflicts of Interest None.

References

1. Bray F, Jemal A, Grey N, Ferlay J, Forman D. Global cancer transitions according to the Human Development Index (2008–2030): a population-based study. Lancet Oncol. 2012;13(8):790–801. doi:10.1016/S1470-2045(12)70211-5.
2. Mackiewicz-Wysocka M, Pankowska M, Wysocki PJ. Progress in the treatment of bone metastases in cancer patients. Expert Opin Investig Drugs. 2012;21(6):785–95. doi:10.1517/13543784.2012.679928.
3. Yu HH, Tsai YY, Hoffe SE. Overview of diagnosis and management of metastatic disease to bone. Cancer Control. 2012;19(2):84–91.
4. Talbot JN, Paycha F, Balogova S. Diagnosis of bone metastasis: recent comparative studies of imaging modalities. Q J Nucl Med Mol Imaging. 2011;55(4):374–410.
5. Murtz P, Krautmacher C, Traber F, Gieseke J, Schild HH, Willinek WA. Diffusion-weighted whole-body MR imaging with background body signal suppression: a feasibility study at 3.0 Tesla. Eur Radiol. 2007;17(12):3031–7.
6. Even-Sapir E, Metser U, Mishani E, Lievshitz G, Lerman H, Leibovitch I. The detection of bone metastases in patients with high-risk prostate cancer: 99mTc-MDP planar bone scintigraphy, single- and multi-field-of-view SPECT, 18F-fluoride PET, and 18F-fluoride PET/CT. J Nucl Med. 2006;47(2):287–97.
7. Schirrmeister H, Buck A, Guhlmann A, Reske SN. Anatomical distribution and sclerotic activity of bone metastases from thyroid cancer assessed with F-18 sodium fluoride positron emission tomography. Thyroid. 2001;11(7):677–83. doi:10.1089/105072501750362754.
8. Schirrmeister H, Glatting G, Hetzel J, Nussle K, Arslandemir C, Buck AK, et al. Prospective evaluation of the clinical value of planar bone scans, SPECT, and 18F-labeled NaF PET in newly diagnosed lung cancer. J Nucl Med. 2001;42(12):1800–4.

9. Schirrmeister H, Guhlmann A, Elsner K, Kotzerke J, Glatting G, Rentschler M, et al. Sensitivity in detecting osseous lesions depends on anatomic localization: planar bone scintigraphy versus 18F PET. J Nucl Med. 1999;40(10):1623–9.
10. Daldrup-Link HE, Franzius C, Link TM, Laukamp D, Sciuk J, Jurgens H, et al. Whole-body MR imaging for detection of bone metastases in children and young adults: comparison with skeletal scintigraphy and FDG PET. AJR Am J Roentgenol. 2001;177(1):229–36.
11. Grant FD, Fahey FH, Packard AB, Davis RT, Alavi A, Treves ST. Skeletal PET with 18F-fluoride: applying new technology to an old tracer. J Nucl Med. 2008;49(1):68–78. doi:10.2967/jnumed.106.037200.
12. Abe K, Sasaki M, Kuwabara Y, Koga H, Baba S, Hayashi K, et al. Comparison of 18FDG-PET with 99mTc-HMDP scintigraphy for the detection of bone metastases in patients with breast cancer. Ann Nucl Med. 2005;19(7):573–9. doi:10.1007/Bf02985050.
13. Kong F-L, Yang DJ. Amino acid transporter-targeted radiotracers for molecular imaging in oncology. Curr Med Chem. 2012;19(20):3271–81. doi:10.2174/092986712801215946.
14. Christensen HN. Role of amino acid transport and countertransport in nutrition and metabolism. Physiol Rev. 1990;70(1):43–77.
15. McGivan JD, Pastor-Anglada M. Regulatory and molecular aspects of mammalian amino acid transport. Biochem J. 1994;299(Pt 2):321–34.
16. Oxender DL, Christensen HN. Evidence for two types of mediation of neutral and amino-acid transport in Ehrlich cells. Nature. 1963;197:765–7.
17. Kanai Y, Segawa H, Miyamoto K, Uchino H, Takeda E, Endou H. Expression cloning and characterization of a transporter for large neutral amino acids activated by the heavy chain of 4F2 antigen (CD98). J Biol Chem. 1998;273(37):23629–32.
18. Yanagida O, Kanai Y, Chairoungdua A, Kim DK, Segawa H, Nii T, et al. Human L-type amino acid transporter 1 (LAT1): characterization of function and expression in tumor cell lines. Biochim Biophys Acta. 2001;1514(2):291–302.
19. Nawashiro H, Otani N, Shinomiya N, Fukui S, Ooigawa H, Shima K, et al. L-type amino acid transporter 1 as a potential molecular target in human astrocytic tumors. Int J Cancer. 2006;119(3):484–92. doi:10.1002/Ijc.21866.
20. Goudarzi B, Kishimoto R, Komatsu S, Ishikawa H, Yoshikawa K, Kandatsu S, et al. Detection of bone metastases using diffusion weighted magnetic resonance imaging: comparison with C-11-methionine PET and bone scintigraphy. Magn Reson Imaging. 2010;28(3):372–9. doi:10.1016/j.mri.2009.12.008.
21. Tomiyoshi K, Amed K, Muhammad S, Higuchi T, Inoue T, Endo K, et al. Synthesis of isomers of F-18-labelled amino acid radiopharmaceutical: position 2- and 3-L-F-18-alpha-methyltyrosine using a separation and purification system. Nucl Med Commun. 1997;18(2):169–75. doi:10.1097/00006231-199702000-00013.
22. Inoue T, Tomiyoshi K, Higuichi T, Ahmed K, Sarwar M, Aoyagi K, et al. Biodistribution studies on L-3-[fluorine-18]fluoro-alpha-methyl tyrosine: a potential tumor-detecting agent. J Nucl Med. 1998;39(4):663–7.
23. Inoue T, Shibasaki T, Oriuchi N, Aoyagi K, Tomiyoshi K, Amano S, et al. 18F-alpha-methyl tyrosine PET studies in patients with brain tumors. J Nucl Med. 1999;40(3):399–405.
24. Kaira K, Oriuchi N, Shimizu K, Ishikita T, Higuchi T, Imai H, et al. Correlation of angiogenesis with 18F-FMT and 18F-FDG uptake in non-small cell lung cancer. Cancer Sci. 2009;100(4):753–8. doi:10.1111/j.1349-7006.2008.01077.x.
25. Miyakubo M, Oriuchi N, Tsushima Y, Higuchi T, Koyama K, Arai K, et al. Diagnosis of maxillofacial tumor with L-3-[F-18]-fluoro-alpha-methyltyrosine (FMT) PET: a comparative study with FDG-PET. Ann Nucl Med. 2007;21(2):129–35.
26. Miyashita G, Higuchi T, Oriuchi N, Arisaka Y, Hanaoka H, Tominaga H, et al. 18F-FAMT uptake correlates with tumor proliferative activity in oral squamous cell carcinoma: comparative study with 18F-FDG PET and immunohistochemistry. Ann Nucl Med. 2010;24(8):579–84. doi:10.1007/s12149-010-0398-2.
27. Kaira K, Oriuchi N, Imai H, Shimizu K, Yanagitani N, Sunaga N, et al. Prognostic significance of L-type amino acid transporter 1 (LAT1) and 4F2 heavy chain (CD98) expression in stage I pulmonary adenocarcinoma. Lung Cancer. 2009;66(1):120–6. doi:10.1016/j.lungcan.2008.12.015.
28. Kaira K, Oriuchi N, Otani Y, Shimizu K, Tanaka S, Imai H, et al. Fluorine-18-alpha-methyltyrosine positron emission tomography for diagnosis and staging of lung cancer: a clinicopathologic study. Clin Cancer Res. 2007;13(21):6369–78. doi:10.1158/1078-0432.Ccr-07-1294.
29. Sato N, Inoue T, Tomiyoshi K, Aoki J, Oriuchi N, Takahashi A, et al. Gliomatosis cerebri evaluated by F-18 alpha-methyl tyrosine positron-emission tomography. Neuroradiology. 2003;45(10):700–7. doi:10.1007/s00234-003-1057-2.
30. Inoue T, Koyama K, Oriuchi N, Alyafei S, Yuan Z, Suzuki H, et al. Detection of malignant tumors: whole-body PET with fluorine 18 alpha-methyl tyrosine versus FDG – preliminary study. Radiology. 2001;220(1):54–62.
31. Watanabe H, Inoue T, Shinozaki T, Yanagawa T, Ahmed AR, Tomiyoshi K, et al. PET imaging of musculoskeletal tumours with fluorine-18 alpha-methyltyrosine: comparison with fluorine-18 fluorodeoxyglucose PET. Eur J Nucl Med Mol Imaging. 2000;27(10):1509–17. doi:10.1007/s002590000344.
32. Wiriyasermkul P, Nagamori S, Tominaga H, Oriuchi N, Kaira K, Nakao H, et al. Transport of 3-fluoro-L-alpha-methyl-tyrosine by tumor-upregulated L-type amino acid transporter 1: a cause of the tumor uptake in PET. J Nucl Med. 2012;53(8):1253–61. doi:10.2967/jnumed.112.103069.
33. Watanabe H, Shinozaki T, Yanagawa T, Aoki J, Tokunaga M, Inoue T, et al. Glucose metabolic analysis of musculoskeletal tumours using 18fluorine-FDG PET as an aid to preoperative planning. J Bone Joint Surg Br. 2000;82(5):760–7.
34. Fujimoto R, Higashi T, Nakamoto Y, Hara T, Lyshchik A, Ishizu K, et al. Diagnostic accuracy of bone metastases detection in cancer patients: comparison between bone scintigraphy and whole-body FDG-PET. Ann Nucl Med. 2006;20(6):399–408.
35. Rosen RS, Fayad L, Wahl RL. Increased F-18-FDG uptake in degenerative disease of the spine: characterization with F-18-FDG PET/CT. J Nucl Med. 2006;47(8):1274–80.
36. Costelloe CM, Murphy WA, Chasen BA. Musculoskeletal pitfalls in F-18-FDG PET/CT: pictorial review. AJR Am J Roentgenol. 2009;193(3):S25–30. doi:10.2214/Ajr.07.7138.
37. Hamaoka T, Madewell JE, Podoloff DA, Hortobagyi GN, Ueno NT. Bone imaging in metastatic breast cancer. J Clin Oncol. 2004;22(14):2942–53. doi:10.1200/jco.2004.08.181.
38. Qu XH, Huang XL, Yan WL, Wu LM, Dai KR. A meta-analysis of 18FDG-PET-CT, 18FDG-PET, MRI and bone scintigraphy for diagnosis of bone metastases in patients with lung cancer. Eur J Radiol. 2012;81(5):1007–15. doi:10.1016/j.ejrad.2011.01.126.
39. Stecco A, Lombardi M, Leva L, Brambilla M, Negru E, Delli Passeri S, et al. Diagnostic accuracy and agreement between whole-body diffusion MRI and bone scintigraphy in detecting bone metastases. Radiol Med. 2013;118(3):165–75. doi:10.1007/s11547-012-0870-2.
40. Hsu W, Hearty TM. Radionuclide imaging in the diagnosis and management of orthopaedic disease. J Am Acad Orthop Surg. 2012;20(3):151–9. doi:10.5435/JAAOS-20-03-151.
41. Ghanem N, Uhl M, Brink I, Schafer O, Kelly T, Moser E, et al. Diagnostic value of MRI in comparison to scintigraphy, PET, MS-CT and PET/CT for the detection of metastases of bone. Eur J Radiol. 2005;55(1):41–55. doi:10.1016/j.ejrad.2005.01.016.
42. Peng X, Guo W, Ren T, Lou Z, Lu X, Zhang S, et al. Differential expression of the RANKL/RANK/OPG system is associated with

bone metastasis in human non-small cell lung cancer. PLoS One. 2013;8(3):e58361. doi:10.1371/journal.pone.0058361.

43. Chatterjee S, Frew J, Mott J, McCallum H, Stevenson P, Maxwell R, et al. Variation in radiotherapy target volume definition, dose to organs at risk and clinical target volumes using anatomic (computed tomography) versus combined anatomic and molecular imaging (positron emission tomography/computed tomography): intensity-modulated radiotherapy delivered using a tomotherapy Hi Art machine: final results of the VortigERN study. Clin Oncol (R Coll Radiol). 2012;24(10):e173–9. doi:10.1016/j.clon.2012.09.004.
44. Lucas JD, O'Doherty MJ, Wong JCH, Bingham JB, McKee PH, Fletcher CDM, et al. Evaluation of fluorodeoxyglucose positron emission tomography in the management of soft-tissue sarcomas. J Bone Joint Surg Br. 1998;80(3):441–7. doi:10.1302/0301-620x.80b3.8232.